Ann. Phys. (Berlin) **526**, No. 9–10, 423–429 (2014) / DOI 10.1002/andp.201400079

annalen der physik

Formation and diffusion characteristics of Pt clusters on Graphene, 1H-MoS_2 and 1T-TaS_2

H. Duygu Ozaydin[1], Hasan Sahin[2,], R. Tugrul Senger[1], and Francois M. Peeters[2]*

Received 16 April 2014, revised 27 May 2014, accepted 27 May 2014
Published online 18 June 2014

Many experiments have revealed that the surfaces of graphene and graphene-like structures can play an active role as a host surface for clusterization of transition metal atoms. Motivated by these observations, we investigate theoretically the adsorption, diffusion and magnetic properties of Pt clusters on three different two-dimensional atomic crystals using first principles density functional theory. We found that monolayers of graphene, molybdenum disulfide (1H-MoS_2) and tantalum disulfide (1T-TaS_2) provide different nucleation characteristics for Pt cluster formation. At low temperatures, while the bridge site is the most favorable site where the growth of a Pt cluster starts on graphene, top-Mo and top-Ta sites are preferred on 1H-MoS_2 and 1T-TaS_2, respectively. Ground state structures and magnetic properties of Pt_n clusters ($n = 2,3,4$) on three different monolayer crystal structures are obtained. We found that the formation of Pt_2 dimer and a triangle-shaped Pt_3 cluster perpendicular to the surface are favored over the three different surfaces. While bent rhombus shaped Pt_4 is formed on graphene, the formation of tetrahedral shaped clusters are more favorable on 1H-MoS_2 and 1T-TaS_2. Our study of the formation of Pt_n clusters on three different monolayers provides a gateway for further exploration of nanocluster formations on various surfaces.

1 Introduction

Graphene, the monolayer honeycomb structure of carbon atoms [1, 2], has been attracting a lot of interest due to its remarkable structural, electronic and thermal properties [3–7]. In addition to the unique properties of graphene, some works have concentrated on the absorption of alkali, noble and transition metals on graphene [8–13]. The attachment of metal nanoparticles to graphene surfaces is a very challenging problem with possible application for electrocatalysis. Regarding the growth of metal clusters on graphene, in particular the formation of platinum nanoclusters is important due to their excellent catalytic behavior [14–16]. In addition, when Pt_n clusters are formed on graphene the equilibrium structure of the gas-phase of the clusters is preserved [14] and magnetic anisotropy energies (MAE) are strongly reduced as compared to free clusters [15]. Theoretical studies have also shown that depending on the growth conditions Pt_n nanostructures with diverse structural symmetries can be formed on graphene [14–17].

Moreover, recent advances in the synthesis of single layer graphene and the understanding of it's unique properties have provided a ground for many other two-dimensional materials such as e.g. transition metal dichalcogenides (TMDs) [18–21]. Following the successful experimental observation of single layers of molybdenum disulfide (MoS_2) [18] synthesis of various TMDs such as WS_2 [22], $MoSe_2$ [23, 24], WSe_2 [25] and ReS_2 [26, 27] have been achieved. Studies revealed that monolayers of TMDs, which are composed of a transition metal atoms sandwiched between chalcogen layers, can exist in two different forms: 1H and 1T phases, and under certain conditions transitions can occur between them [28, 29]. Owing to their various phases and atomic structures, TMDs show a wide range of electronic, mechanical, chemical and thermal characteristics [29–32].

Formation of clusters of large atoms on various substrates and their size dependent electronic and magnetic properties have been investigated intensively during the past twenty years. Optical properties of Ag cluster films on mylar and mica substrates were investigated experimentally [40]. In addition, the effect of the atomic

* Corresponding author Email: hasan.sahin@uantwerpen.be
[1] Department of Physics, Izmir Institute of Technology, 35430 Izmir, Turkey
[2] Department of Physics, University of Antwerp, 2610 Antwerp, Belgium

radius on the Sn_n and Pb_n cluster structures was investigated theoretically [41]. Moreover, magnetic impurities in small metallic clusters were investigated theoretically and the correlations between the cluster structure and the magnetic behavior were revealed [42].

Similar to graphene, TMDs form weakly bonded lamellar bulk structures and these van der Waals layers can host intercalation of foreign atoms and the formation of various clusters. Aydinol et al. investigated theoretically the intercalation properties of various lithium-metal-oxides, sulfides, and selenides [33]. Ramirez and Schkatte performed a detailed study of the migration and energetics of Li adatoms on a $TiSe_2(0001)$ surface and showed that notwithstanding the high energy barrier, direct intercalation can be possible [34]. Jishi et al. showed that the electronic density of states in $TiSe_2$ can be significantly enhanced upon copper intercalation [35]. Furthermore, Meziane et al. calculated Li and Na intercalation in dichalcogenides of Tantalum and found that they are promising candidates for thermoelectric applications [36]. Experimentally, Kim et al. reported that MoS_2 and WS_2 can be decorated with gold atoms and the resulting gold nanoparticles tend to grow at defective sites and the resulting MoS_2/Au and WS_2/Au hybrid structures show significant enhanced electrocatalytic performance towards hydrogen evolution reactions [37]. Moreover, Sreeprasad et al. demonstrated the possibility of raising the effective gate-voltage of MoS_2 devices by an order of magnitude through the incorporation of highly capacitive gold nanoparticles onto the surface [38]. Very recently the successful functionalization of graphene membranes with platinum nanoparticles that tend to exhibit a preferred orientation was reported by Xu et al [39].

Although structural, electronic and magnetic properties of freestanding and graphene-supported Pt_n clusters were investigated before, only very few studies are available on cluster formation on surfaces of various TMDs having different crystal symmetry. In this paper, motivated by the very recent experimental realizations of monolayer TMDs, we investigate: (i) what are the migration characteristics of Pt atoms on different monolayer surfaces, and (ii) how TMD substrates having different crystal symmetries affect the formation of Pt_n nanoclusters ($n < 5$).

The paper is organized as follows: In Sec. 2 we give details of our computational methodology. In Sec. 3 adsorption and diffusion characteristics of single Pt atom on monolayers of graphene, MoS_2 and TaS_2 are presented. In Sec. 4 our results on the binding energies and magnetic properties of Pt_2, Pt_3 and Pt_4 nanostructures on three different surfaces are given. Our results are discussed in Sec. 5.

2 Computational methodology

The structural optimization and adsorption characteristics of Pt_n clusters on graphene, MoS_2, and TaS_2 sheets reported here are based on density functional theory in the framework of the plane-wave projector-augmented wave (PAW) methodology implemented in the Vienna *ab-initio* simulation package VASP [43, 44]. The Perdew-Burke-Ernzerhof (PBE) [45] form of the Generalized Gradient Approximation (GGA) were adopted to describe electron exchange and correlation.

For Pt_n clusters on graphene, MoS_2 and TaS_2 sheets, calculations were performed using $5 \times 5 \times 1$ supercells which are large enough to avoid interactions between neighboring clusters. The plane-wave cutoff energy was set to 500 eV in all calculations. The Brillouin Zone was sampled using a Γ-centered k-point mesh and a Gaussian smearing of 0.01 eV is used for total energy calculations. Structural relaxations were performed using a conjugate gradient method where total energy and atomic forces are minimized. The convergence criteria for energy was chosen as 10^{-5} eV between two iteration steps, and the maximum force allowed on each atom was less than 10^{-4} eV/Å. The pressure in the unit cell was held below 1 kBar in the optimized structures. Spin-polarized calculations were performed in all cases and atomic charges were calculated by using the Bader method [46, 47].

Previous studies have shown that the first principles methodology is a quite powerful tool for the understanding of structures and magnetic ordering of atomic clusters and various stacking types. The role of the electronic distribution on the magnetic properties and structural modulation was successfully predicted by Wang et al [48]. In addition Xu et al [49]. demonstrated that the oscillation of the Ni magnetic moment that depends on the atomic shuffling in the superstructure dominates the distribution of the total magnetic moment per Ni_2MnGa unit. Similarly, the investigation of crystallographic and magnetic structures of the Ni2XGa (where X=Mn, Fe, Co) showed that the value and the alignment of the local magnetic moments sensitively depend on the interatomic distances [50]. In addition, it was experimentally and theoretically shown that stacked bilayers of Pd/C60 are ferromagnetic and the observed ferromagnetism originates from the formation Pd clusters between the bilayers [51].

Table 1 Calculated parameters for Pt_n clusters on graphene, 1H-MoS_2 and 1T-TaS_2 respectively; stable configurations for the Pt_n-cluster/substrate systems, total magnetic moment of the cluster M_{total} (μ_B), binding energy per Pt atom E_b (eV/atom) and the average charge transfered between the surface and the Pt cluster $\Delta\rho$. Positive values of $\Delta\rho$ correspond to charge donation to the Pt cluster.

	Graphene				1H-MoS_2				1T-TaS_2			
	Shape	M_{total} (μ_B)	E_b (eV/atom)	$\Delta\rho$ (e)	*Shape*	M_{total} (μ_B)	E_b (eV/atom)	$\Delta\rho$ (e)	*Shape*	M_{total} (μ_B)	E_b (eV/atom)	$\Delta\rho$ (e)
Pt_1	-	0.0	1.70	0.02	-	0.0	2.89	−0.07	-	1.0	3.71	−0.10
Pt_2	Dimer	0.0	2.25	−0.02	Dimer	0.0	3.03	−0.07	Dimer	0.1	3.68	−0.01
Pt_3	Triangle	0.0	2.97	−0.03	Triangle	0.0	3.35	0.08	Triangle	1.0	3.87	0.16
Pt_4	Bent Rhombus	2.0	3.15	−0.11	Tetrahedral	0.0	3.60	0.03	Tetrahedral	0.3	4.01	0.21

For the determination of the most favorable adsorption sites calculations were performed by placing Pt single atoms over various high symmetry lattice points. In Table 1, only the energetically most favorable sites were reported. The binding energies (per Pt atom) were calculated according to the formula $E_b = [E(Host) + nE(Pt) - E(Host + Pt_n)]/n$, where $E(Host)$ is the energy of the supporting monolayer sheet, $E(Host + Pt_n)$ is the total energy of the monolayer with Pt atom(s), $E(Pt)$ is the energy of an isolated Pt atom and n is the number of Pt atoms in the cluster.

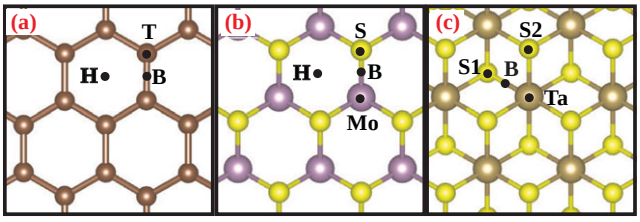

Figure 1 (Color online) Top views of the atomic structures of (a) graphene, (b) 1H-MoS_2 and (c) 1T-TaS_2 and possible adsorption sites: the hollow site (H), the bridge site (B), the top-Mo site (Mo) and the top-Ta site (Ta). S1 and S2 refer to the point on top of a S atom of upper and lower chalcogen layers in 1T-TaS_2, respectively.

3 Adsorption and migration of single Pt atom

In this section, we present our results concerning favored adsorption sites, the binding energies and magnetic ground states for a single Pt atom on monolayers of graphene, MoS_2 and TaS_2. Just like graphene, MoS_2 and TaS_2 have hexagonal crystal structure composed of layers of metal atoms (M) sandwiched between layers of chalcogen atoms (X) with stoichiometry MX_2. As shown in Fig. 1, while MoS_2 has trigonal prismatic coordination, each Ta atom has octahedral coordination in monolayer TaS_2. In the following discussion, trigonal prismatic and octahedral phases are referred as 1H and 1T structures, respectively. In both H and T phases the trigonally arranged monolayer lattice of metal atoms is sandwiched between two chalcogen layers and hence each metal atom is surrounded by six chalcogen atoms. In contrast to the weak inter-layer interaction, metal and chalcogen atoms have strong intra-planar bonds that have a covalent character. Due to different lattice symmetries of these monolayers one can expect different diffusion characteristics for foreign atoms on these different surfaces. Our results are summarized in Table I. Diffusion pathways (see Fig. 2) of a Pt atom on different supporting layers were obtained by calculating the total energy on different adsorption sites along the high symmetry points.

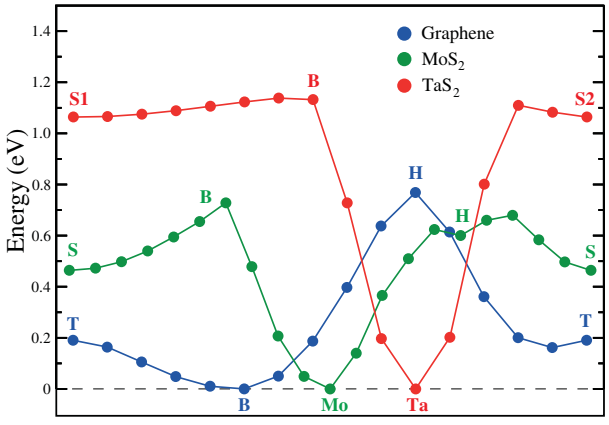

Figure 2 Variation of energy for a single Pt adatom along the symmetry points (shown in Fig. 1) of single layer graphene, MoS_2 and TaS_2. Zero of energy is set to the energy of the most favorable site.

The calculated lattice constant of the primitive unit-cell of graphene is $a = 2.46$ Å. For adsorption calculations of a single platinum atom on a non-defective surface a 4×4 graphene supercell is used. As shown in Fig. 1(a) there are three favorable adsorption sites on the surface of graphene: the hollow (H) site on the center of a hexagon, the bridge (B) site on the midpoint of a C-C bond, and the top (T) site directly above a carbon atom. In agreement with recent *ab initio* calculations the bridge site is found to be the energetically most favorable site. Each Pt atom is adsorbed at the B site with binding energy of 1.70 eV. Although, an isolated platinum is in a magnetic ground state with 2 μ_B net moment, when it is adsorbed on graphene there exists no net magnetic moment. This finding is consistent with the previously reported data [8]. Our analysis reveals that the nonmagnetic state is favored by 0.92 meV over the magnetic state with 2 μ_B net moment.

Differing from the one-atom-thick crystal structure of graphene, MoS_2 has a three-layered structure made of trigonally arranged Mo atoms sandwiched by two S layers. The point group of graphene is D_{6h}, while the monolayer (1H) structure of MoS_2 belongs to the D_{3h} symmetry group. We found that the optimized lattice constant of 1H-MoS_2 is 3.18 Å and a 3×3 supercell is large enough to hinder the interaction between Pt atoms in adjacent cells. For the adsorption of a single Pt atom on 1H-MoS_2 there are four different possible sites: on top of Mo (Mo), on top of S (S), on top of a Mo-S bond (B) and on top of the hollow (H) sites (see Fig. 1(b)). When a Pt atom is adsorbed at the Mo site, the largest binding energy (minimum total energy) is found. It is also seen that immersion of a Pt atom to the Mo layer is not allowed at the hollow site by an energy barrier of 6.91 eV. Therefore, the most stable site of Pt atom absorption occurs at the Mo site with a binding energy of 2.89 eV.

Similar to MoS_2, TaS_2 monolayer contains 3 layers of octahedrally coordinated S-Ta-S atoms. This monolayer (1T) structure belongs to the symmetry group of D_{3d}. However, differing from 1H-MoS_2, 1T-TaS_2 shows metallic behavior. The optimized lattice constant of the 1T-TaS_2 sheet is $a = 3.74$ Å and a 3×3 supercell is used. Calculations of adatom Pt and monolayer TaS_2 system are carried out for the Pt atom located at the four high symmetry sites, as indicated in Fig. 1(c): on bridge (B), on top of S (S1), on top of Ta (Ta) and on top of lower layer S atom (S2). The most favorable site for Pt atom adsorbed on TaS_2 was found to be the Ta site with binding energy of $E_b = 3.71$ eV/atom. Upon the adsorption of a Pt atom on Ta site TaS_2 monolayer exhibits a spin polarized ground state with net magnetic moment of 1 μ_B.

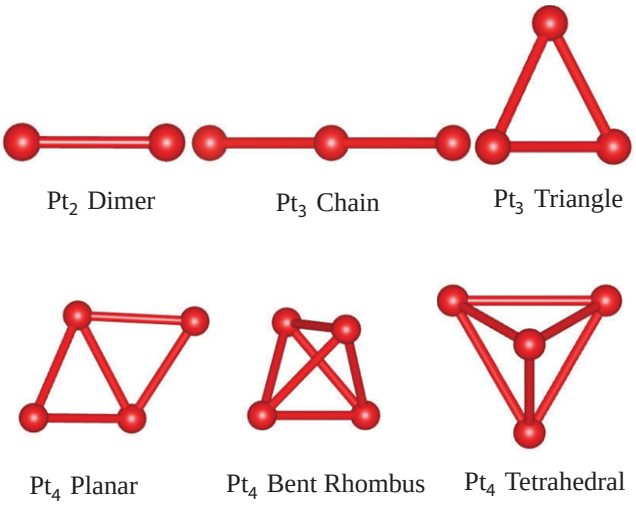

Figure 3 (Color online) Possible configurations of Pt_n clusters on the surface of monolayers of graphene, MoS_2 and TaS_2.

4 Pt_n clusters on different monolayers

In this section the formation of Pt_n clusters on various surfaces were investigated via total energy calculations. In order to accurately simulate the step-by-step nucleation of each Pt_n cluster, various configurations of Pt_{n-1}+Pt systems were considered. As shown in Fig. 3 there are several possible configurations for each Pt_n cluster. Although all the possible configurations of n Pt atoms that correspond to a minimum on the Born-Oppenheimer surface were considered in our calculations, only the atomic structures that correspond to the ground state geometry are presented in Fig. 4 for the sake of clarity.

4.1 Pt_2 clusters

As shown in Fig. 4(a) when a Pt atom is adsorbed on the surface of graphene the most favorable adsorption site for the next Pt atom is found to be a second nearest bridge site. Due to the larger atomic radius of Pt atoms adsorption on the first nearest bridge site is not allowed. For this Pt_2 dimer the Pt-Pt bond length is 2.60 Å and the average Pt-C bond length is 2.15 Å. The binding energy of a Pt_2 dimer is calculated to be 2.25 eV/atom and therefore the formation of each dimer occurs with an energy benefit of 0.55 eV/atom. It is also found that the Pt_2+graphene structure does not exhibit any spin polarization in its ground state.

As depicted in Fig. 4(b), when a Pt atom is adsorbed on MoS_2, neither nearest top-sulfur nor nearest hollow

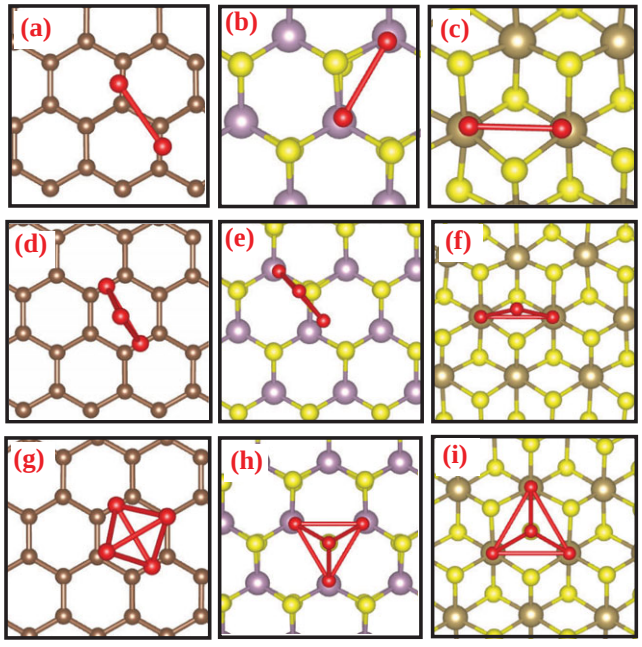

Figure 4 (Color online) Most stable configurations for Pt_n-clusters on three different substrates, graphene (left column), MoS_2 (middle column) and TaS_2 (right column). The red balls denote Pt atoms.

site is the preferential site for the next Pt atom. Differing from the graphene surface, MoS_2 allows dimer formation on nearest top-Mo sites. Therefore a full coverage of the MoS_2 surface by a trigonally arranged one-atom-thick layer of Pt atoms may be possible under suitable conditions. Here the calculated binding energy of a dimer is 3.03 eV/atom and therefore the 0.14 eV/atom energy benefit shows the preferability of clusterization on the MoS_2 substrate. Here the Pt_2+MoS_2 structure has a nonmagnetic ground state. In addition, our charge analysis showed that 0.07 of electrons are transfered from the Pt atoms to the surface whereas charge transfer from the Pt_2 clusters to the graphene surface is 0.02 electrons.

However changing the substrate to TaS_2 results in some differences in energetics and electronic properties of Pt_2 clusters. When Pt_2 clusters are formed on the TaS_2 sheet the distance between Pt-Pt is 2.85 Å and the Pt-S distance is 2.32 Å. The binding energy is $E_b = 3.68$ eV/atom and Pt atoms are both located on top of the Ta sites (see Fig. 4(c)). Although the most favorable configuration of two Pt atoms is a dimer as on the MoS_2 surface, the ground state is spin polarized with a net magnetic moment of 0.1 μ_B. Another significant difference between the two TMDs, MoS_2 and TaS_2, is that the formation of Pt_2-dimers is not energetically favorable on TaS_2. It appears that the decoration of TaS_2 by Pt atoms may provide quite stable surface structures with new functionalities.

4.2 Pt_3 clusters

For a Pt_3 cluster supported by single layer graphene, the energetically most stable form is a triangle-shaped cluster perpendicular to the surface. In this configuration two Pt atoms sit on opposite B sites and the other Pt is located at the hollow site (see Fig. 4(d)). We have also considered flat-lying triangle and linear chain configurations which turned out to have higher energy. Since these two structures are not energetically favorable, thermal effects immediately drive the atoms to form a triangle-shaped Pt_3 structure perpendicular to the surface. Consequently, clustering is favored since the binding energy is E_b=2.97 eV/atom. The Pt atoms, which are located at the C-C bridge sites, have bonding length 2.46 Å , and the Pt-C bond length is 2.24 Å. Due to the weak interaction between them, it is nonmagnetic and 0.03 electrons are transfered from the surface to the Pt cluster.

As discussed above for graphene, we treated both linear chain and triangular shapes for Pt_3 clusters on MoS_2 layer. The same behavior is shown by the Pt_3-cluster adsorbed on MoS_2. The system is inclined to form a nearly perpendicular triangle with binding energy of 3.35 eV/atom, which is depicted in Fig. 4(e). No significant magnetic moments are induced on the 5×5 MoS_2 layer. The average bond length of the Pt atoms is about 2.67 Å, and the length of the nearest Pt-S bond is 2.26 Å. The system is nonmagnetic and charge transfer occurs from the surface to the Pt_3 clusters (0.08 electrons).

On the other hand, three Pt atoms on a TaS_2 layer appear magnetic with a net magnetic moment of 1 μ_B. The configuration shown in Fig. 4(f) displays a triangular shaped Pt_3 on graphene or MoS_2, but the distance between the Pt-Pt atoms located on the Ta site is much longer and therefore the Pt-Pt interaction is weak. However the interaction between the cluster and the TaS_2 layer is quite strong. The two platinum atoms which sit on top of the Ta atoms have a bond length of 3.31 Å, and the distance to the other Pt atom is 2.51 Å, however the bond length with the surface is about 2.37 Å. From the Bader analysis, it appears that 0.16 electrons are given from the surface to the Pt_3 cluster.

4.3 Pt_4 clusters

For the case of Pt_4, there are three typical structures that can be formed on a surface; planar, bent rhombus or

tetrahedral as shown in Fig. 3. The bent rhombus cluster on graphene (see Fig. 4(g)) is more favorable than the flat one with an energy difference of 66 meV/atom. In this configuration the length of the shortest Pt-Pt bond is 2.52 Å, and the Pt-C bond is about 2.23 Å. While the single Pt atom, the most stable Pt_2 and Pt_3 clusters on graphene are nonmagnetic, Pt_4 has a ferromagnetic ground state with a net magnetic moment of 2 μ_B. It appears that 0.11 of electron charge are transported from the Pt atoms to the surface.

For four Pt atoms adsorbed on the MoS_2 surface, the most favored configuration state consists of a three dimensional tetrahedral shape where three Pt atoms are located on top of Mo, and the fourth Pt atom is bonded to the other three Pt atoms only (Fig. 4(h)). The average distance between the edge platinum atoms and sulfur atoms is 2.35 Å and the binding energy of the cluster is E_b= 3.60 eV/atom. The plane configuration of Pt_4 is not a stable state. The Pt_4 cluster adsorbed on the MoS_2 structure has a nonmagnetic ground state and the charge transfer from the surface to the adatom Pt is 0.03 electrons.

Finally, we analyzed the structural and magnetic properties of Pt_4 clusters on a TaS_2 sheet. We have compared the adsorption energies of a planar and a tetrahedron structure. Not surprisingly as shown in Fig. 4(i), after relaxation the Pt_4 clusters exhibit a tetrahedral shape on TaS_2 because it is 0.7 eV more favorable than the planar shape. The Pt-Pt bond length of the edge atoms is 3.54 Å while the average distance to the S atoms is 2.37 Å. For the system of Pt_4+TaS_2, the magnetic properties are also investigated, and it has a degenerate ground state consisting of nonmagnetic and magnetic cases with 2 μ_B. Moreover, charge transfer from the TaS_2 to Pt_4 cluster is 0.21 electrons.

5 Conclusions

We investigated the adsorption properties, the diffusion pathways and clustering of Pt atoms on graphene, 1H-MoS_2 and 1T-TaS_2 by means of density functional theory. While a single Pt atom is adsorbed on the bridge site of graphene, the top of the transition metal atom is the most favorable site on TMD substrates. It is also seen that the binding energies on TMDs are larger on 1H-MoS_2 and 1T-TaS_2. Our total energy calculations also revealed that the formation of Pt_n clusters is favorable on graphene, MoS_2 and TaS_2 substrates. We found that these substrates, with their different crystal symmetries, exhibit different absorption and diffusion characteristics. While graphene hosts an easy clusterization of Pt atoms, nucleation of Pt clusters on the surface of transition metal dichalcogenides, regardless of the 1H or 1T phase, is more difficult and can take place at higher temperatures. Due to the larger atomic separation on 1T-TaS_2 one can expect a smaller mobility of the clusters. We believe that our study on monolayer crystals having different symmetries provide a gateway for further exploration of nanocluster formations on various surfaces.

Acknowledgement. This work was supported by the Flemish Science Foundation (FWO-Vl) and the Methusalem foundation of the Flemish government. Computational resources were provided by TUBITAK ULAKBIM, High Performance and Grid Computing Center (TR-Grid e-Infrastructure). H.S. is supported by a FWO Pegasus Long Marie Curie Fellowship.

Key words. two-dimensional materials, graphene, MoS2, TaS2, monolayers.

References

[1] K. S. Novoselov, A. K. Geim, S. V. Morozov, D. Jiang, M. I. Katsnelson, I. V. Grigorieva, S. V. Dubonos, and A. A. Firsov, Nature **438**, 197 (2005).
[2] K. S. Novoselov, A. K. Geim, S. V. Morozov, D. Jiang, Y. Zhang, S. V. Dubonos, I. V. Grigorieva, and A. A. Firsov, Science **306**, 666 (2004).
[3] A. A. Balandin, Nature Materials **10**, 569 (2011).
[4] A. K. Geim and K.S. Novoselov, Nature Materials **6**, 183 (2007).
[5] A. K. Geim, Science **324**, 1530 (2009).
[6] A. H. Castro Neto, F. Guinea, N.M.R. Peres, K. S. Novoselov, and A. K. Geim, Rev. Mod. Phys. **81**, 109 (2009).
[7] S. Cahangirov, C. Ataca, M. Topsakal, H. Sahin, and S. Ciraci, Phys. Rev. Lett. **108**, 126103 (2012).
[8] H. Sahin and S. Ciraci, J. Phys. Chem. C **116**(45) 24075 (2012).
[9] I. Cabria, M. J. Lopez, and J. A. Alonso, Phys. Rev. B **81**, 035403 (2010).
[10] A. Ishii, M. Yamamoto, H. Asano, and K. Fujiwara, J. Phys.: Conf. Ser. **100**, 052087 (2008).
[11] B. Uchoa, C.-Y. Lin, and A. H. Castro Neto, Phys. Rev. B **77**, 035420 (2008).
[12] K. T. Chan, J. B. Neaton, and M. L. Cohen, Phys. Rev. B **77**, 235430 (2008).
[13] O. V. Yazyev and A. Pasquarello, Phys. Rev. B **82**, 045407 (2010).
[14] P. Blonski, S. Dannler, and J. Hafner, J. Chem. Phys. **134**, 034107 (2011).
[15] P. Blonski and J. Hafner, J. Chem. Phys. **134**, 154705 (2011).
[16] Z. Zhou, F. Gao, and W. Goodman, Surf. Sci. **604**, L31 (2010).

[17] M. N. Huda, Manish K. Niranjan, B. R. Sahu, and L. Kleinman, Phys. Rev. A **73**, 053201 (2006).
[18] K. S. Novoselov, D. Jiang, F. Schedin, T. J. Booth, V. V. Khotkevich, S. V. Morozov, and A. K. Geim, Proc. Natl. Acad. Sci. USA **102**, 10451 (2005).
[19] R. A. Gordon, D. Yang, E. D. Crozier, D. T. Jiang, and R. F. Frindt, Phys. Rev. B **65**, 125407 (2002).
[20] J. N. Coleman, M. Lotya, A. O'Neill, S. D. Bergin, P. J. King, U. Khan, K. Young, A. Gaucher, S. De, R. J. Smith, I. V. Shvets, S. K. Arora, J. J. Boland, J. J. Wang, J. F. Donegan, J. C. Grunlan, G. Moriarty, A. Shmeliov, R. J. Nicholls, J. M. Perkins, E. M. Grieveson, K. Theuwissen, D. W. Mc Comb, P. D. Nellist, V. Nicolosi, Science **331**, 568 (2011).
[21] Q. H. Wang, K. Kalantar-Zadeh, A. Kis, J. N. Coleman, and M. S. Strano, Nature Nanotech. **7**, 699 (2012).
[22] J. S. Ross, P. Klement, A. M. Jones, N. J. Ghimire, J. Yan, D. G. Mandrus, T. Taniguchi, K. Watanabe, K. Kitamura, W. Yao, D. H. Cobden, and X. Xu, Nature Nanotech. **9**, 268 (2014).
[23] S. Tongay, J. Zhou, C. Ataca, K. Lo, T. S. Matthews, J. Li, J. C. Grossman, and J. Wu, Nano Letters **12**, 5576 (2012).
[24] S. Horzum, H. Sahin, S. Cahangirov, P. Cudazzo, A. Rubio, T. Serin, and F. M. Peeters, Phys. Rev. B **87**, 125415 (2013).
[25] H. Sahin, S. Tongay, S. Horzum, W. Fan, J. Zhou, J. Li, J. Wu, and F. M. Peeters, Phys. Rev. B **87**, 165409 (2013).
[26] S. Tongay, H. Sahin, C. Ko, A. Luce, W. Fan, K. Liu, J. Zhou, Y.-S. Huang, C.-H. Ho, J. Yan, D. F. Ogletree, S. Aloni, J. Ji, S. Li, J. Li, F. M. Peeters, and J. Wu, Nature Comm. **5**, 3252 (2014).
[27] S. Horzum, D. Cakir, J. Suh, S. Tongay, Y.-S. Huang, C.-H. Ho, J. Wu, H. Sahin, and F. M. Peeters, Phys. Rev. B **89**, 155433 (2014).
[28] M. Chhowalla, H. S. Shin, G. Eda, L.-J. Li, K. P. Loh, and H. Zhang, Nature Chem. **5**, 263 (2013).
[29] C. Ataca, H. Sahin, and S. Ciraci, J. Phys. Chem. C **116**, 8983 (2012).
[30] H. Wang, L. Yu, Y.-H. Lee, Y. Shi, M. L. Chin, L.-J. Li, M. Dubey, J. Kong, and T. Palacios, Nano Lett. **12**, 4674 (2012).
[31] Y. J. Zhang, J. T. Ye, Y. Matsuhashi, and Y. Iwasa, Nano Lett. **12**, 1136 (2012).
[32] H. Fang, S. Chuang, T. C. Chang, K. Takei, T. Takahashi, and A. Javey, Nano Lett. **12**, 3788 (2012).
[33] M. K. Aydinol, A. F. Kohan, and G. Ceder, Phys. Rev. B **56**, 1354 (1997).
[34] C. Ramirez and W. Schattke, Surface Science **482**, 424 (2001).
[35] R. A. Jishi and H. M. Alyahyaei, Phys. Rev. B **78**, 144516 (2008).
[36] S. Meziane, H. Feraoun, T. Ouahrani, C. Esling, Journal of Alloys and Compounds **581** (2013).
[37] J. Kim, S. Byun, A. J. Smith, J. Yu, and J. Huang, J. Phys. Chem. Lett. **4**, 1227 (2013).
[38] T. S. Sreeprasad, P. Nguyen, N. Kim, and V. Berry, Nano Lett. **13**, 4434 (2013).
[39] P. Xu, L. Dong, M. Neek-Amal, M. Ackerman, J. Yu, S. Barber, J. Schoelz, D. Qi, F. Xu, P.M. Thibado, and F. M. Peeters, ACS Nano **8**, 2697 (2014).
[40] S. Nepijko, W. Schulze, I. Rabin, and L. Viduta, Ann. Physik **510**(2), 101, (1998).
[41] B. Wang, L. M. Molina, M. J. Lopez, A. Rubio, J. A. Alonso, and M. J. Stott, Ann. Physik **7**(2), 107, (1998).
[42] G. M. Pastor, Ann. Physik **14**(9), 547 (2005).
[43] G. Kresse and J. Furthmller, Comp. Mat. Sci. **6**, 15 (1996); Phys. Rev. B 54, 11169 (1996).
[44] G. Kresse and D. Joubert, Phys. Rev. B **59**, 1758 (1999).
[45] J. P. Perdew, K. Burke, and M. Ernzerhof, Phys. Rev. Lett. **77**, 3865 (1996).
[46] R. F. W. Bader, Atoms in Molecules - A Quantum Theory, Oxford University Press, Oxford, (1990).
[47] G. Henkelman, A. Arnaldsson, and H. Johnson, Comput. Mater. Sci. **36**, 354 (2006).
[48] X. Wang, J.-X. Shang, F.-H. Wang, C.-B. Jiang, and H.-B. Xu, JMMM, **355**, 173 (2014).
[49] N. Xu, J.-M. Raulot, Z. Li, J. Bai, Y. Zhang, X. Zhao, L. Zuo, and C. Esling, Appl. Phys. Lett. **100**, 084106 (2012).
[50] J. Bai, J. M. Raulot, Y. D. Zhang, C. Esling, X. Zhao, and L. Zuo, J. App. Phys. **108**, 064904 (2010).
[51] S. Ghosh, S. Tongay, A. F. Hebard, H. Sahin, and F. M. Peeters, JMMM **349**, 128 (2014).